FISEVIER

Contents lists available at ScienceDirect

Case Studies in Thermal Engineering

journal homepage: www.elsevier.com/locate/csite





Enhancing thermal decomposition in cylindrical reactors: A finite element analysis of thermal aspects and fluid dynamics for thermosensitive, exothermic compounds

Djelloul Bendaho ^a, Zakaria Sari Hassoun ^b, Noureddine Kaid ^c, Sultan Alqahtani ^{d,e}, Younes Menni ^{c,f,g,*}, Ali J. Chamkha ^{h,**}, Badr M. Alshammari ⁱ, Lioua Kolsi ^j

- ^a Institute of Technology, University Center Salhi Ahmed Naama (Ctr. Univ. Naama), P.O. Box 66, Naama, 45000, Algeria
- b MECACOMP Laboratory, Mechanical Engineering Department, Faculty of Technology, Abou-Bekr Belkaid University, P.O. Box 119, 13000, Tlemcen. Algeria
- ^c Energy and Environment Laboratory, Department of Mechanical Engineering, Institute of Technology, University Center Salhi Ahmed Naama (Ctr. Univ. Naama), P.O. Box 66, Naama, 45000, Algeria
- ^d College of Engineering, Mechanical Engineering Department, King Khalid University, Abha, Saudi Arabia
- ^e Center for Engineering and Technology Innovations, King Khalid University, Abha, Saudi Arabia
- ^f College of Technical Engineering, National University of Science and Technology, Dhi Qar, 64001, Iraq
- g Department of Computer Engineering, Biruni University, 34010, Istanbul, Turkey
- h Faculty of Engineering, Kuwait College of Science and Technology, Doha District, 35004, Kuwait
- ⁱ Department of Electrical Engineering, College of Engineering, University of Ha'il, Ha'il City, 81451, Saudi Arabia
- ^j Department of Mechanical Engineering, College of Engineering, University of Ha'il, Ha'il City, 81451, Saudi Arabia

ARTICLE INFO

Keywords: Finite element analysis Laminar flow Thermal decomposition Exothermic reactions Cylindrical reactors

ABSTRACT

_This work numerically investigates the thermal decomposition of compound A in a thermosensitive exothermic cylindrical reactor. The study primarily focuses on the influence of the reactor's configuration and heating temperature on its total performance. Simulations of reactors with 2, 4, 6, and 8 hot cylinders are performed using COMSOL Multiphysics 5.0 and finite element analysis, taking the heating temperatures as 30 °C, 40 °C, and 50 °C using an activation energy of 70 kJ/mol with an initial fluid velocity of 0.001 m/s. The results depicted that at 50 °C, the performance of the 4-cylinder reactor was the best; indeed, the exit concentration of reactant 'A' compared to that in the 2-cylinder reactor was decreased by 20.42 %, and the reaction rate of 25.5 mol/m³.s proved high conversion efficiency along with favorable thermal conditions. The 4cylinder reactor showed better performance against all other reactors, namely the 6-cylinder and 8-cylinder reactors, through both reaction rate and conversion efficiency. Also, the cylinder size variation analysis for the 4-cylinder reactor shows that increasing the radius (Rcyl) of the cylinder from 2 mm to 4 mm gave a higher exit temperature of 56.332 °C, a 74.63 % reduction in the exit concentration of 'A' compared to a cylinder size of 2 mm, while the competitive reaction rate becomes 26.1 mol/m³.s. Although the reaction rate for the 4 mm radius cylinder was somewhat lower than that for the 2 mm radius, the larger size managed heat much more effectively, and the 4-cylinder reactor with a 4 mm radius at 50 °C was the most optimal configuration. This setup provides the best balance of high reaction rates, efficient conversion, and effective thermal

E-mail addresses: menni.younes@cuniv-naama.dz (Y. Menni), achamkha@yahoo.com (A.J. Chamkha).

https://doi.org/10.1016/j.csite.2025.105913

^{*} Corresponding author. Energy and Environment Laboratory, Department of Mechanical Engineering, Institute of Technology, University Center Salhi Ahmed Naama (Ctr. Univ. Naama), P.O. Box 66, Naama, 45000, Algeria.

^{**} Corresponding author.

conditions for thermal decomposition, offering significant insights into reactor design optimization.

1. Introduction

Thermal decomposition refers to an important chemical process whereby any substance changes into simpler substances under a high temperature. The processes are among the important aspects of material science, chemistry, and engineering for the production of nanocomposites. Understanding the mechanisms of reaction, kinetics, generation, waste treatments, and creation of new materials with exceptional properties makes this process useful. Consequently, a wide range of studies were conducted with the aim to optimize mechanisms and kinetics of the thermal decomposition for application purposes, at the same time studying properties and potential uses to extend the use in a variety of technological developments [1,2].

Many of the thermal decomposition processes involve exothermic chemical reactions that may affect the temperature profile and the heat transfer characteristics. It is of paramount importance to understand such complex interactions in optimizing performance and safety in thermal decomposition systems, in particular in non-isothermal tubular flow reactors with cylindrical geometries [3–5]. Steady-state behavior in cylindrical pipes, considering the heat loss to the surroundings, has been the subject of many studies on exothermic reactions [6]. New reactor designs have also been suggested, such as tube-shell type axial tubular reactors, that would ensure much better safety and yield of the product by keeping the reactive mixture away from the high-temperature zone [7]. The analysis of heat transfer and reactant consumption in stockpiles of reactive materials has further elucidated the intricate relationships between temperature, reaction rates, and reactant depletion [8].

Beyond traditional geometries, there are studies that have considered the thermal behavior of functionally graded and thermosensitive hollow cylinders by employing cylindrical-polar coordinate systems to model such complex systems [9]. Various fluid parameters like Lewis numbers, heat radiation, chemical reactions, thermophoresis, Brownian motion, free stream velocity, and the magnetic field were studied for their influence on temperature, nanoparticle concentration, and speed in nanofluids flowing over cylindrical surfaces [10]. Advanced numerical techniques, such as complex-variable transient thermo-mechanical finite elements and complex Taylor series expansion methods, have been developed by the authors for capturing the transient thermal and stress responses in thick-walled cylinders with temperature-dependent material properties [11]. These techniques allow for very accurate sensitivity analyses that provide deep insights into the material, shape, and loading parameters affecting system response.

Numerical simulations have also been used to investigate the flow and heat transfer behavior of viscous nanofluids over stretching cylinders, considering models such as Buongiorno's, in order to analyze the effects produced by different flow control parameters [12]. In addition, the influence of heat sources, thermal radiation, chemical reactions, and natural convection on the flow of Carreau fluids over vertically stretching cylinders immersed in porous media has been analyzed [13]. Besides, the natural convection characteristics of reacting chemicals in square enclosures containing circular cylinders were studied by employing coordinate transformations to map the physical domain to a computational domain [14].

Zhang et al. [15], on the other hand, prepared carbon cryogel-tin oxide nanocomposites with minimal impurities by an impregnation-calcination method based on the thermal decomposition of stannous sulfate for lithium-ion battery anodes. Structural characterizations showed that the tin oxide nanoparticles, which were formed from the decomposition of stannous sulfate, were uniformly distributed within the pores of carbon cryogels. The results demonstrated that carbon cryogels with large specific surface areas, high porosity, and small mesopores facilitate the deposition of tin oxide nanoparticles. Wijayanti et al. [16] investigated the thermal decomposition of macroalgae to produce substances that can serve as alternative fuels, drying the samples to reduce moisture content. Besides this, thermal decomposition studies have led to the development of green propellants and have been used to propose green bipropellant combinations that exhibit excellent energy properties along with good ignition delay characteristics [17]. Addition of N_2O decreased the average ignition delay of energetic ionic liquids; thus, this could lead to a tunable bipropellant system with controlled presence of N_2O .

Thermally driven decomposition processes have been studied within the framework of transformer oil analysis to determine structural changes of mineral oils during their lifetime. The change in the activation energy for the thermal decomposition process has been examined using thermogravimetry after accelerated aging, thus providing significant information on the condition of the oil and overall health of the transformer [18]. In parallel with these studies, efforts have been made toward a better understanding of the underlying thermal decomposition reaction mechanisms. For instance, some studies investigated the silane decomposition in flow reactors and determined the temporal relation of silane consumption and disilane formation, referring to variables like the total hydrogen content and aerosol particle concentration versus fractions of polyhydride groups [19].

Thermal decomposition processes have also been used for the synthesis of monodisperse silver nanoparticles. It was successful to decompose silver-fatty acid complexes at high temperatures in a nitrogen atmosphere into stable monodisperse silver nanoparticles. These have well-characterized size distributions verified by high-resolution transmission electron microscopy and surface-plasmon absorption spectroscopy [20]. Meanwhile, the thermal decomposition behavior was further presented for some polymer blends including the polyamide-6/poly (vinyl chloride) - PVC blends [21]. These studies have provided insight into the mechanism of depolymerization of PA-6, which generates ε -caprolactam and cyclic oligomers, and have been very useful for depicting the recyclability and environmental aspects concerning these materials.

Kohga [22] studied the decomposition and combustion of ammonium nitrate/polytetrahydrofuran propellants with glycerol propoxylate. The catalytic effects of Fe₂O₃, MnO₂, and ammonium dichromate on decomposition and combustion were investigated to

arrive at an improved propellant formulation. Another area of interest has been the production of valued carbon-based materials through waste rubber thermal decomposition. Experimental works have investigated the thermolysis process at high steam temperatures, which resulted in ash residues with properties within the range of commercial carbon blacks [23]. The preparation method still faces problems related to high ash content and high sulfur levels in the resulting materials.

1.1. Research objective

This work investigates and develops the understanding of thermal decomposition mechanisms, with an emphasis on complex interactions between exothermic reactions, fluid dynamics, and heat transfer occurring within non-isothermal tubular reactors and cylindrical geometries relevant to thermal decomposition systems. By understanding these fundamental processes, this study aims at reactor performance optimization in a manner that it not only enhances safety and operational efficiency but also exerts a far greater level of control over product property precision. The general strategy is, therefore, a contribution toward more efficient, reliable, and sustainable thermal decomposition systems with profound design and operational insight.

The Finite Element Method, FEM, is very important in simulating thermal decomposition processes in cylindrical reactors for details of thermal behavior, temperature profiles, and chemical species distribution. This numerical technique is very advanced for modeling complex physical phenomena, as illustrated in the work of Bendaho et al. [24]. FEM can successfully model such complex thermal and chemical behaviors within these reactors to allow the researchers to identify the critical zones, optimize designs, and predict system behavior under different conditions. Our contribution covers the development of an optimum thermal decomposition process in cylindrical reactors by simulating the same key aspects using the FEM technique. We focus on the improvement of reactor design and heat transfer efficiency by strategically placing heated cylinders. This is intended to enhance safety and efficiency in industrial reactors while providing useful information on what the ideal configuration for more efficient and safe industrial processes may be.

1.2. Key innovations in reactor design and optimization

A number of key novelties are given in the work that contribute substantially to reactor design and optimization. Thermal decomposition processes for a number of heated cylinders (2, 4, 6, and 8) and heating temperatures (30 °C, 40 °C, and 50 °C) have been systematically analyzed in this work. It provides the optimal configuration-4 heated cylinders at 50 °C-which strikes a balance between the highest reaction rates, high efficiency of conversion of reactants, and effective thermal management. Further, FEM through COMSOL Multiphysics 5.0 allows comprehensive simulation of thermal and hydrodynamic behavior within the reactor, including temperature profiles, fluid dynamics, and reaction rates. The further investigation into the effect of cylinder size revealed that an increase in cylinder radius results in increased efficiency in the conversion of reactants while maintaining competitive reaction rates-a novel paradigm in optimizing reactor geometry. Lastly, the development of a general-purpose framework in this work applicable to a wide range of thermosensitive, exothermic reactions renders the present findings of value in such diversified areas as material science, chemical engineering, and energy storage.

2. Modeling and simulation

2.1. Chemical formulation

Arrhenius' law, proposed in 1889, describes the exponential relationship between the rate of a chemical reaction and temperature (Eq. (1)).

$$k = A \cdot e^{\frac{-E}{RT}} \tag{1}$$

Where,

k: Reaction rate constant (s^{-1}),

T: Absolute temperature (K).

A: Pre-exponential factor (universal constant for ideal gases) (J/mol.K),

E: Activation energy (J/mol),

R: Gas constant (8.314 J/mol.K).

In an aqueous environment, heat-sensitive compound 'A' decomposes into smaller fragments 'B' through an unimolecular reaction:

$$A_{(in water)} \rightarrow B (fragments)$$
 (2)

When exposed to heat in a water-based system, compound 'A' decomposes into fragments 'B'.

The reaction rate, which depends on the kinetics and thermodynamics of the process, is expressed in mol/m³.s as:

$$rate = k.c_{A} \tag{3}$$

Here, c_A represents the concentration of compound 'A'.

The thermal decomposition reaction is exothermic, releasing energy. The rate of this energy release, denoted as Q, can be calculated using:

$$Q = -rate \times H \tag{4}$$

Where the *rate* denotes the reaction velocity and H stands for the heat of reaction, specifically noted here as (-100 kJ/mol). This equation allows for the quantification of the energy released during the thermal decomposition process.

2.2. Mathematical formulations and boundary conditions

In single-phase flow modeling, the Navier-Stokes equations lead to a compressible continuity equation:

$$\frac{\partial \rho}{\partial t} + \nabla \cdot (\rho u) = 0 \tag{5}$$

and the equation of momentum:

$$\rho \frac{\partial u}{\partial t} + \rho u \cdot \nabla u = -\nabla p + \nabla \cdot \left(\mu \left(\nabla u + (\nabla u)^T \right) - \frac{2}{3} \mu (\nabla u) I \right) + F$$
(6)

Where

 μ : Dynamic viscosity (N.s/m²),

u: Velocity (m/s),

 ρ : Fluid density (kg/m³),

p: Pressure (Pa),

F: Body force term (N/m^3) .

In this model, the steady-state condition eliminates the first term in each equation. The following table summarizes the boundary conditions that were made use of in modeling the fluid flow within this system. Velocity boundary conditions comprising no-slip conditions, inlet velocity, and outlet pressure (see Table 1).

The energy balance equation for the reactor accounts for convection and conduction:

$$\rho C_p(u.\nabla)T + \nabla \cdot (-\lambda \nabla T) = Q \tag{7}$$

In above, C_p the specific heat capacity (J/kg.K), λ the thermal conductivity (W/m.K), and the term Q signifies a heat source (W/m³). At the inlet and heating cylinder surface, the temperature boundary conditions are:

$$T = T_0 \tag{8a}$$

$$T = T_{cyl} \tag{8b}$$

At the outlet, an outflow boundary condition is set, where energy passes through via convective transport, and the conduction heat flux is zero:

$$q_{cond}$$
, $n = -\lambda \Delta T$, $n = 0$ (9)

The resulting equation for total heat flux is

$$q.n = \rho.C_{\rm n}.T.u.n \tag{10}$$

Assume no energy transfer across the reactor plates:

$$q.n = 0 \tag{11}$$

Mass transfer in the reactor domain follows the stationary convection-diffusion equation

$$\nabla \cdot (-D_i \nabla c_i) + u \cdot \nabla c_i = R_i \tag{12}$$

 D_i is the diffusion coefficient (m²/s) while R_i is the reaction term (mol/m³.s). This equation assumes that the species i is diluted in a solvent.

The boundary conditions, including the inlet concentration, outlet mass transport, and insulation boundaries, are detailed in Table 2.

Table 1 Velocity boundary conditions.

Boundary condition	Description	Equation
Inlet velocity Outlet pressure No-slip condition	Velocity component in the direction of the normal vector at the boundary. Zero-pressure condition at the outlet Fluid velocity at the boundary matches the velocity of the boundary surface (typically zero).	$u.n = u_0$ $P = P_{atm}$ $u = 0$

Table 2Mass transport boundary conditions.

Boundary condition	Description	Equation
Inlet concentration Outlet mass transport	Concentration of compound A at the inlet Mass transport primarily through convection at the outlet with negligible diffusion	$c_i = c_{i,0}$ $n.(-D_i \nabla c_i) = 0$ $N_i.n = c_i u.n$
Insulation boundary condition	No mass transport across the boundary on the reactor plates and heating cylinder surfaces	$N_i.n = 0$

2.3. Modeling

Simulation presented below refers to thermal decomposition of a compound 'A' in thermosensitive exothermic cylindrical reactor described in Fig. 1. The strong influence of both reactor geometry and heating temperature was emphasized, and in-depth analysis of the reactor performance for various conditions has been given.

COMSOL Multiphysics 5.0 simulations and finite element analysis are performed for reactors with 2, 4, 6 and 8 hot cylinders at heating temperatures of 30 $^{\circ}$ C, 40 $^{\circ}$ C and 50 $^{\circ}$ C with activation energy of 70 kJ/mol. The inlet velocity is maintained at 0.001 m/s, while the cylinder radius (R_{cyl}) is fixed at 3 mm.

Following the selection of the optimal reactor configuration, the second part of the study examined the effect of cylinder size, with radii (R_{cyl}) of 2 mm, 3 mm, and 4 mm (see Fig. 2).

In this study, water (with dissolved compound 'A') enters the computational domain at 25 °C. Its properties are assumed to represent the entire fluid ($\rho = 997 \text{ kg/m}^3$, $\mu = 8.90 \times 10^{-4} \text{ Pa s}$, $\lambda = 0.606 \text{ W/m.K}$, $C_p = 4180 \text{ J/kg.K}$, and $D_i = 2.0 \times 10^{-9} \text{ m}^2/\text{s}$). The Reynolds number (Re) is derived from input property values, indicating flow behavior.

$$Re = \frac{\rho vd}{\mu} = \frac{997 \times 0.001 \times 0.008}{8.9 \times 10^{-4}} \approx 9 \tag{13}$$

In this study, the Re number is calculated using the specified property values at the reactor inlet. For the analysis, a flow velocity of 0.001 m/s and a characteristic diameter d of 0.008 m are chosen. When the channel is rectangular and the flow is primarily determined by its inlet, the hydraulic diameter is given by $d = \frac{4^{\circ}Area}{Perimeter}$. In cases where the channel width is significantly larger than d (e.g., in a 2D approximation where the width is effectively infinite), the hydraulic diameter simplifies to d because the perimeter is predominantly influenced by the height.

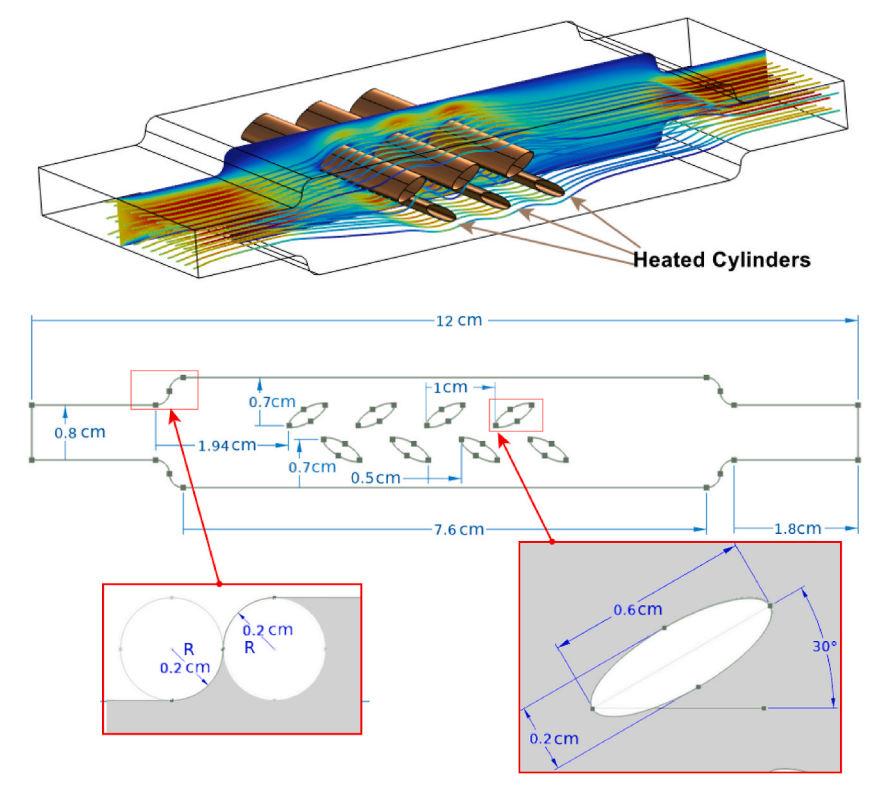


Fig. 1. Reactor geometry with heated cylinders.

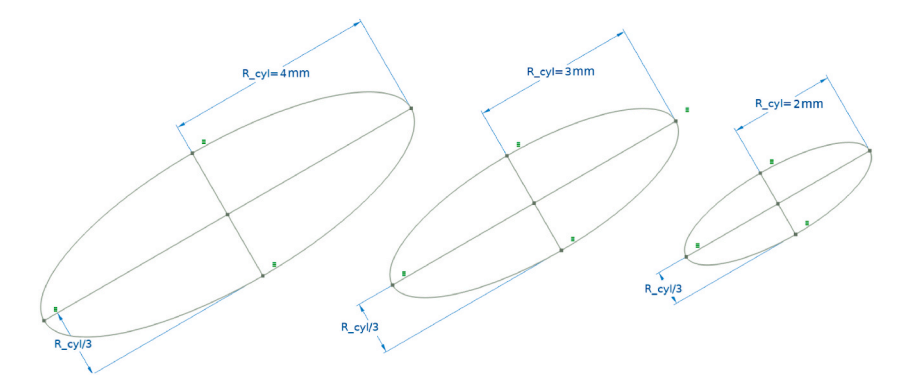


Fig. 2. Studied cylinder dimensions.

Chemical processes depend on fluid dynamics and temperature gradients, with mass transport relying on velocity (u) from the momentum equation (Eq. (6)):

$$\frac{\partial c_i}{\partial t} + \nabla \cdot (-D_i \nabla c_i + c_i u) = R_i \tag{14}$$

 R_i depends on temperature, which is the dependent variable in the energy transport equation:

$$\rho C_p \frac{\partial T}{\partial t} + \nabla \cdot (-\lambda \nabla T) + \rho C_p u \cdot \nabla T = Q$$
(15)

The reaction rate is a function of the type of reactants, their concentration, and collision theory. In a reaction of $A \rightarrow B$, the concentration of 'A' decreases while that of 'B' increases; its rate is defined as a change in its concentration, see Eq. (16).

$$Velocity = \frac{\Delta[B]}{\Delta t} = -\frac{\Delta[A]}{\Delta t}$$
 (16)

In this study, the mathematical formulations, boundary conditions, and physical properties are derived from the COMSOL 5.0 Multiphysics documentation.

2.4. Numerical implementation

Numerical solution of the governing equations was made by means of COMSOL Multiphysics 5.0, while the spatial domain was discretized into small elements by the FEM; these elements were in tetrahedral form, as depicted in Fig. 3. At each of these elements, the unknown variables (temperature, velocity, and concentration) are approximated by appropriate polynomial interpolation functions. The Galerkin method is then applied in order to convert the partial differential equations into a system of algebraic equations that can be solved numerically. In the current study, energy and momentum transport equations have been addressed by coupling the 'Heat Transfer Module' and 'CFD Module' available in COMSOL, while the interface 'Transport of Diluted Species' has been used for modeling mass transport and reaction kinetics. A direct solver was used, namely the PARDISO, to solve the resulting system of equations. Mesh independence studies were performed to ensure the accuracy of the solution. The convergence criterion was set to

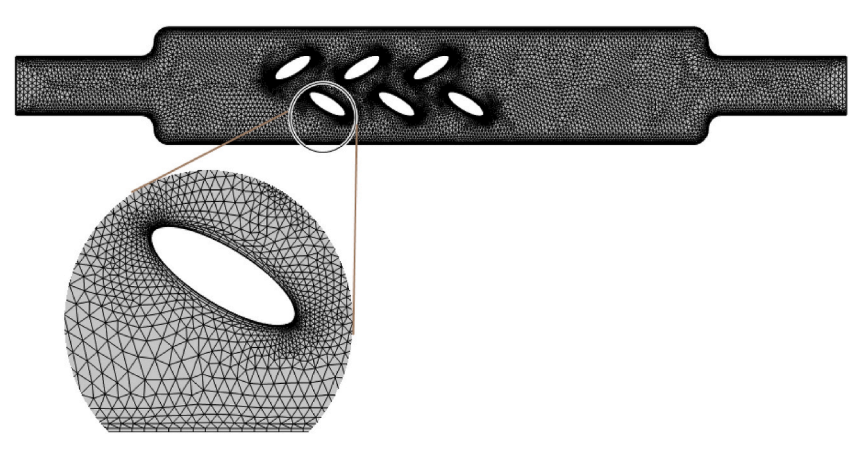


Fig. 3. Detail of finite element mesh.

 10^{-4} for all variables.

2.5. Mesh independence

The meshing strategy in this study is crucial to obtain accurate and reliable results of the simulation. The tetrahedral mesh was chosen for the good representation it can make of the complex geometry of the reactor, including the cylindrical heating elements. Mesh refinement has been done near the cylinder surfaces and wall surfaces where high gradients of temperature and velocity are expected. Fig. 3 shows a detailed finite element mesh of the computational domain that accurately represents the geometrical intricacies and features of the model. The zoomed view shows the refinement in the mesh around critical regions, especially around the orifices. The approach of careful meshing allowed the exact resolution of physical phenomena in question and enabled a good analysis of the flow dynamics as well as heat transfer characteristics.

Fig. 4 shows the distribution of the local Nusselt number (*Nu*) along the x-coordinate for the adiabatic upper wall of the reactor for the following mesh resolutions: 155,044; 104,720; 44,064; and 22,142 elements. The Nusselt number (*Nu*) is a dimensionless parameter that represents the ratio of convective to conductive heat transfer across a boundary. For a cylindrical reactor, the local Nusselt number can be calculated using the following formula:

$$Nu = (h.d)/\lambda \tag{17}$$

Where,

h is the convective heat transfer coefficient $(W/m^2.K)$,

d is the characteristic diameter of the cylinder (m),

 λ is the thermal conductivity of the fluid (W/m.K).

Increasing mesh resolution refines the local *Nu* number profile, capturing finer heat transfer details. Convergence of profiles with higher resolutions indicates a more accurate numerical solution. The curves for 155,044 and 104,720 elements coincide closely, so a resolution of 104,720 elements was deemed sufficiently accurate.

3. Results and discussion

3.1. Hydrodynamic aspects

Fig. 5a–d depicts the velocity vectors in the reactor with two heated cylinders, Fig. 5a; four cylinders, Fig. 5b; six cylinders, Fig. 5c; and eight cylinders, Fig. 5d. The temperature of all cylinders is kept constant at 50 °C and with an activation energy of 70 kJ/mol. According to the hydrodynamic boundary conditions, the inlet flow velocity is kept constant at 0.001 m/s. The flow lines are straight for a length of 1.8 m from the reactor inlet, after which the local fluid velocity shows variations as it enters the expanded zone in the reactor and approaches the cylinders. The fluid possesses the highest velocity at the inlet and outlet parts of the reactor, having a value of approximately 14×10^{-4} m/s, while it decreases towards the walls of the reactor and the cylinders. At the downstream of the cylinders, small recirculation zones can be seen, which is indicative of the secondary flows inside the reactor. These secondary flows are very important in the dynamics of the reactor because they enhance mixing considerably-a very important factor for performance improvement in this type of reactor.

The presence of secondary flows and recirculation zones enhances better mixing and reaction rates within the reactor. This improved mixing results in a more homogeneous distribution of reactants and, therefore, enhances the general efficiency of the

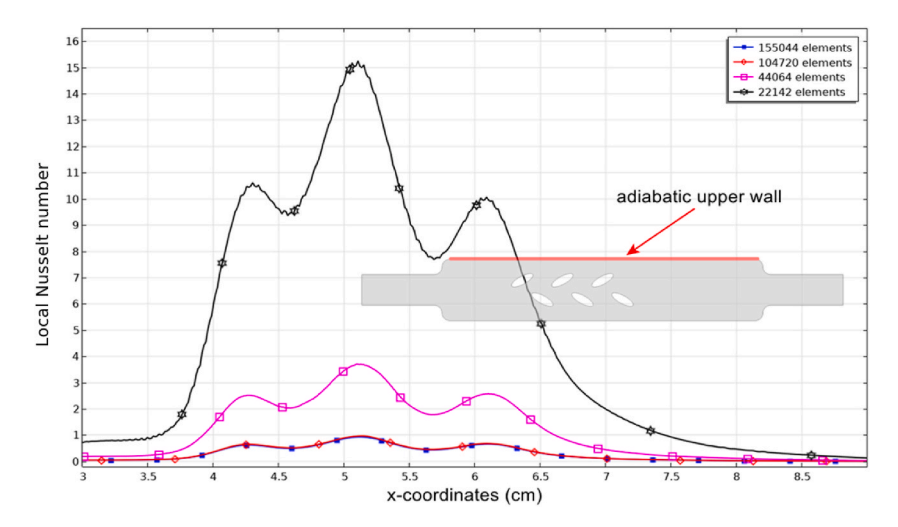


Fig. 4. Local Nusselt number distribution along the reactor's adiabatic upper wall for various mesh resolution.

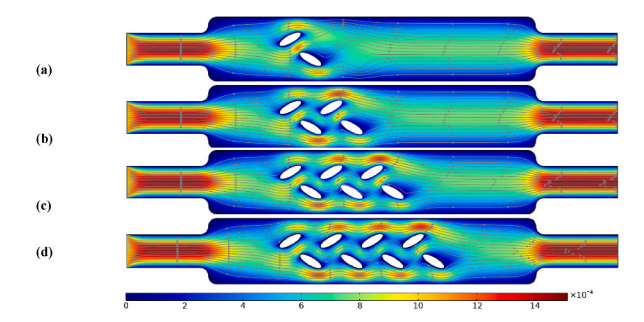


Fig. 5. Velocity vectors (m/s) in different reactor models: (a) Two, (b) Four, (c) Six, and (d) Eight cylinders ($R_{cyl} = 3$ mm, E = 70 kJ/mol, $V_0 = 0.001$ m/s).

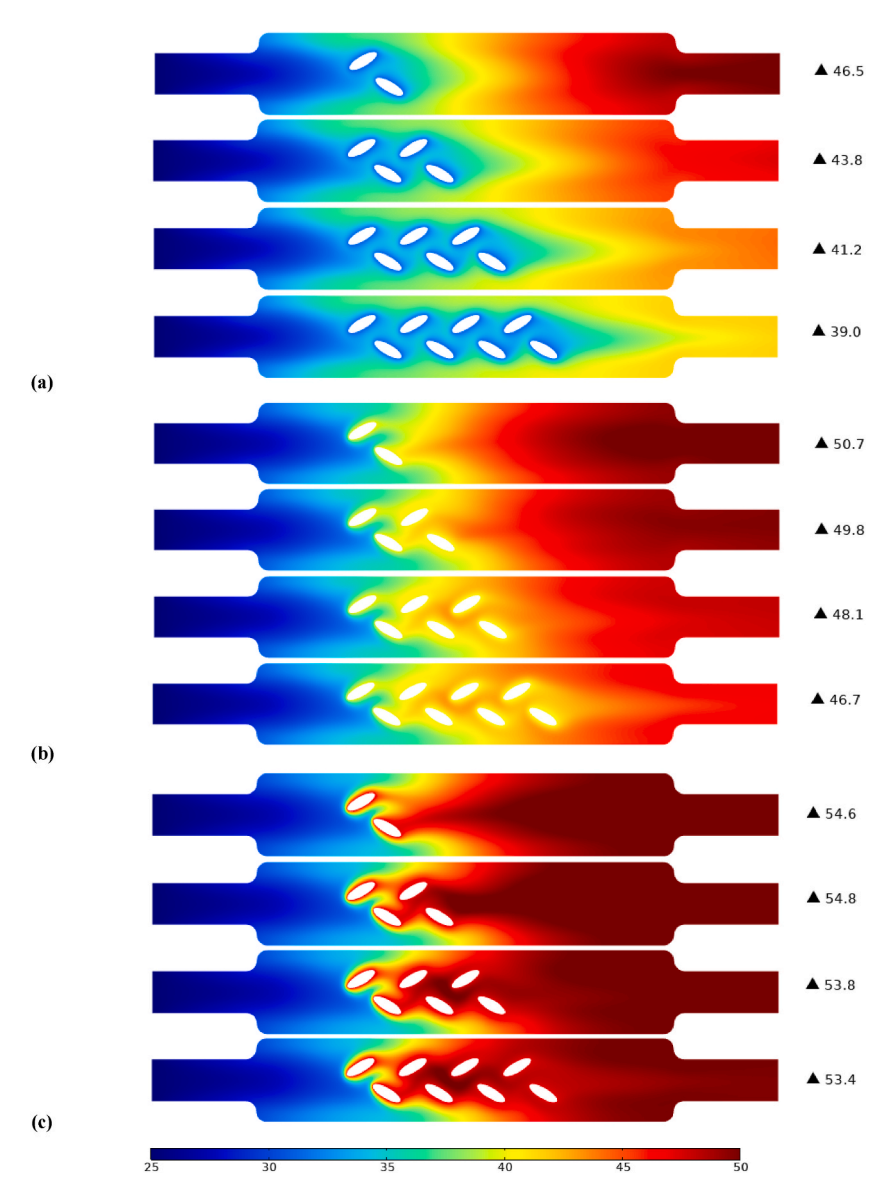


Fig. 6. Temperature distribution (°C) in reactor models with cylinder temperatures: (a) 30 °C, (b) 40 °C, and (c) 50 °C ($R_{cyl}=3$ mm, E=70 kJ mol $^{-1}$, $V_0=0.001$ m $^{-1}$ s $^{-1}$, exothermic reaction).

process. The possibility of these secondary flows to promote better contact between the reactants underlines their importance for an optimum reactor performance and therefore is an integral part of the design and operation of heated cylinder reactors.

3.2. Thermal aspects

From the described process, the temperature patterns inside the reactor due to the exothermic nature of the reaction influence substantially on the general temperature distribution. Fig. 6a, b, and 6c represent the temperature distribution when the cylinder temperature is $30\,^{\circ}$ C, and $50\,^{\circ}$ C, respectively, at all cylinders of R = 3 mm radius. In all cases considered, the reactor temperature developed is noticeably higher due both to the heating and to the exothermic reaction itself. Temperature increases near the cylinders and increases further along the second half of the reactor. Moreover, when the temperature of the cylinders increased from $30\,^{\circ}$ C to $50\,^{\circ}$ C, the reactor's temperature further improved. Conversely, at increased numbers of cylinders from 2 to 8, the reactor temperature decreases for cylinder temperatures of $30\,^{\circ}$ C and $40\,^{\circ}$ C.

With two cylinders at the minimum temperature of 30 $^{\circ}$ C in the cylinders, the reactor temperature is raised to 46.5 $^{\circ}$ C, an increase of 86 $^{\circ}$ relative to the 25 $^{\circ}$ C inlet fluid temperature and 55 $^{\circ}$ M increase compared to the cylinder temperature. Using four cylinders resulted in a temperature of the reactor at 43.8 $^{\circ}$ C. These represented increases of 75.2 $^{\circ}$ M with regard to the inlet fluid and 46 $^{\circ}$ M relating to the cylinder temperature. With six cylinders, the reactor temperature is about 41.2 $^{\circ}$ C, which corresponds to an increase of 64.8 $^{\circ}$ M and 37.3 $^{\circ}$ M, respectively. For eight cylinders, the reactor temperature is about 39 $^{\circ}$ C, which is 56 $^{\circ}$ M higher than the inlet fluid temperature and 30 $^{\circ}$ M higher than the cylinder temperature.

At an average cylinder temperature of 40 $^{\circ}$ C, the reactor temperature varies in the range between 46.7 $^{\circ}$ C and 50.7 $^{\circ}$ C. This corresponds to increases of 86.8 %–102.8 % with regard to the inlet fluid temperature and 16.8 %–26.8 % with regard to the cylinder temperature. For the maximum cylinder temperature of 50 $^{\circ}$ C, the reactor temperature ranges between 53.4 $^{\circ}$ C and 54.8 $^{\circ}$ C. These values represent increases of 113.6 %–119.2 % compared to the inlet fluid temperature and improvements of 6.8 %–9.6 % compared to the cylinder temperature.

Comparing the effect of different cylinder configurations gives significant insights about the thermal behavior of the reactor. At the

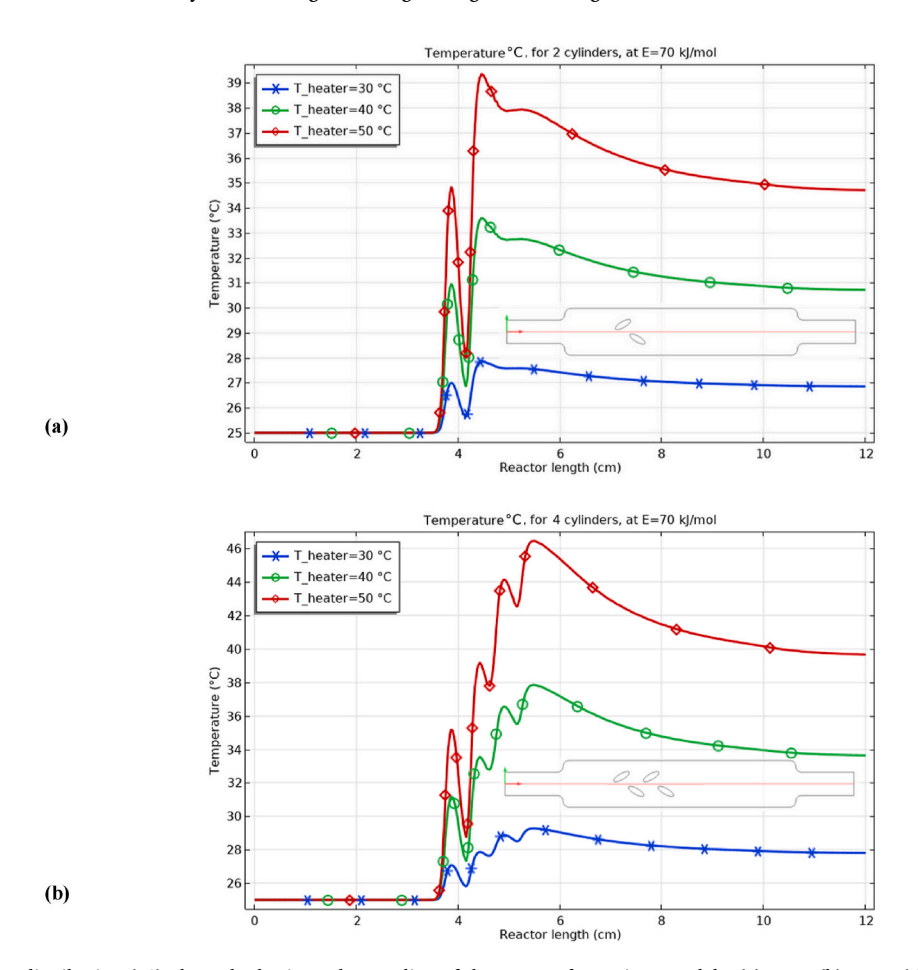
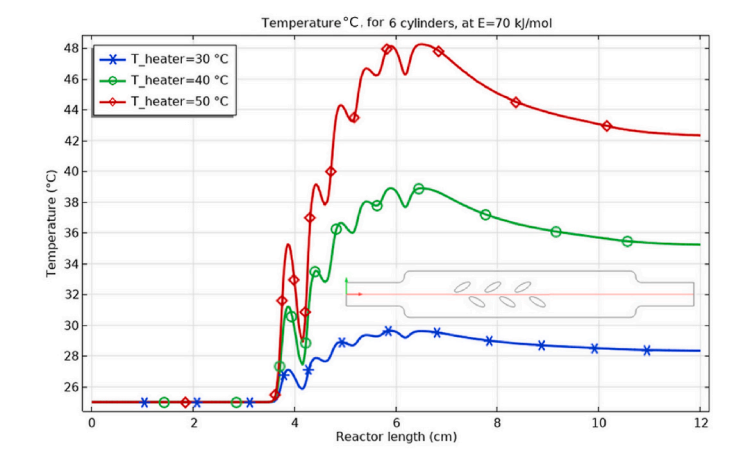


Fig. 7. Temperature distribution (°C) along the horizontal centerline of the reactor for various models: (a) Two, (b) Four, (c) Six, and (d) Eight cylinders (Heating only, excluding heat from exothermic reaction).

(c)



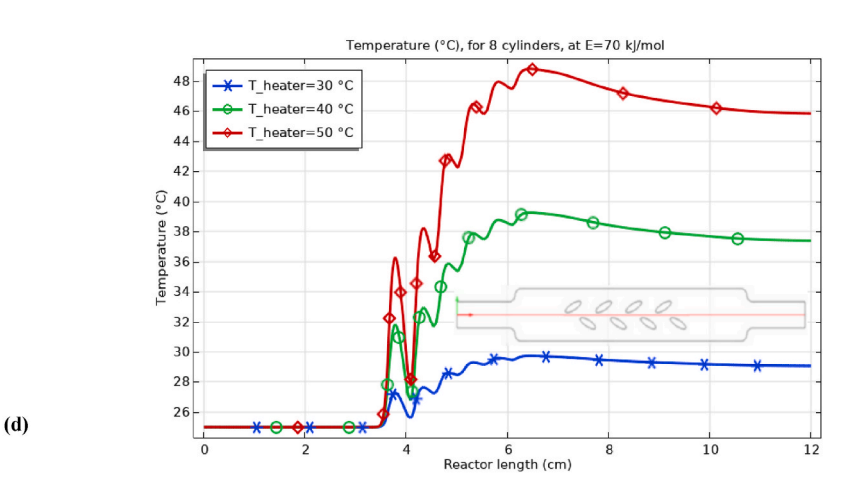


Fig. 7. (continued).

lowest heating temperature of 30 $^{\circ}$ C, the two-cylinder reactor condition gave the highest reactor temperature, improving by about 6.16 %, 12.86 %, and 19.3 % compared to the four-cylinder, six-cylinder, and eight-cylinder reactor configurations, respectively. This suggests that fewer cylinders with a lower temperature promote a larger increase in reactor temperature because of reduced thermal dissipation and thus more concentrated heat generation due to the exothermic reaction. At the mean heating temperature of 40 $^{\circ}$ C, the two-cylinder reactor condition still presented the best thermal performance, improving reactor temperatures about 1.80 %, 5.40 %, and 8.56 % over the four-cylinder, six-cylinder, and eight-cylinder reactor configurations, respectively. The reason may be that even with moderate heating, the higher local temperature rise is contributed by fewer cylinders, leveraging exothermic reactions coupled with heating. However, this trend changes when the heating temperature increases to the highest value of 50 $^{\circ}$ C, and the maximum increase in reactor temperature is realized for the four-cylinder reactor condition. Specifically, this setup provided an increase in temperature of about 0.36 % from the two-cylinder reactor, 1.85 % from the six-cylinder reactor, and 2.62 % from the eight-cylinder reactor. This would indicate that at higher heating temperatures, a medium number of cylinders creates the ideal balance between heat diffusion and the contribution of the exothermic reaction for the reactor to reach its maximum temperature.

The temperature profiles, along the horizontal centerline of the reactor, shown in Fig. 7a–d, depict the thermal effects from the heated cylinders alone, excluding any influence from the exothermic reaction. In all cases, the temperature of the fluid stays at $25\,^{\circ}$ C along the first $3.5\,$ cm from the entrance to the reactor because the heating walls are absent there, implying a thermal equilibrium. Beyond this point, the temperature gradients start changing due to the heat transfer from the heated cylinders. The maximum fluid temperature in the two-cylinder reactor model is achieved at about $4.5\,$ cm from the inlet. This temperature peaks at $28\,^{\circ}$ C when there is minimum heating of the cylinder at $30\,^{\circ}$ C, $33.6\,^{\circ}$ C when there is medium heat at $40\,^{\circ}$ C, and $39.5\,^{\circ}$ C when at maximum heating at $50\,^{\circ}$ C. After this thermal peak, the temperature decreases further along the reactor and stabilizes at the outlet at $26.9\,^{\circ}$ C, $30.7\,^{\circ}$ C, and $34.7\,^{\circ}$ C, respectively, for the three heating scenarios of $30\,^{\circ}$ C, $40\,^{\circ}$ C, and $50\,^{\circ}$ C. This gradual decrease in temperature shows that the effect of the hot cylinders weakens as the fluid moves forward and the dissipation of heat is more pronounced. In the configuration of the four cylinders, the maximum temperature achieved was at a slightly longer distance from the inlet at around $5.5\,$ cm, but at peak temperatures of $29\,^{\circ}$ C for $30\,^{\circ}$ C heated, $38\,^{\circ}$ C for the $40\,^{\circ}$ C, and $46.5\,^{\circ}$ C for $50\,^{\circ}$ C heated cylinders respectively. Again similar to the two-

cylinder model, the temperature decreases gradually during the progress of the fluid toward the reactor outlet. The fluid temperature decreases as it proceeds further away from the heating cylinders and stabilizes when it reaches the outlet position. Other reactor models have similar thermal behavior, but with differences in temperature gradients. With more cylinders, as in the six- and eight-cylinder models, the temperature of the fluid next to the cylinders rises, further enhancing the overall reactor temperature.

Fig. 8 show the fully developed temperature profile including the exothermic reaction. Comparing these plots again can be very instructive for gaining insight into exactly how the reaction alters the temperature distribution that was set up by the geometry of the cylinders. For all of the configurations, the first 3.5 cm from the inlet, the fluid temperature increases slightly from 25 °C to 31 °C. This slight increase indicates that very little reaction activity was present in this zone and there is no important release of thermal energy. This phenomenon is consistent for all reactor models and under various heating conditions. Outside this zone, the reactor temperature increases significantly within the heated cylinders zone. The increased rate of reaction here raises the energy release and increases the overall thermal energy of the reaction. This temperature increase continues until it stabilizes at the reactor outlet, consistent across all reactor configurations. Overall, the liquid temperature varies in direct correlation with the heating temperature of the cylinders within the reactor.

Fig. 9 illustrates the temperature distribution at the reactor exit for different models and heated cylinder temperatures. The temperature of the fluid at the outlet clearly varies with the number of heated cylinders and the heating temperature. There is a noticeable difference among the various examined cases. At the lowest heating temperature of 30 °C, the overall temperature of the reactor increases as the number of cylinders decreases from 8 to 2. The configuration with 2 cylinders resulted in the lowest heating requirement while releasing the most thermal energy from the decomposition reaction, thereby enhancing thermal behavior. In this optimal case, the outlet temperature reached 46.5 °C, which is an improvement of approximately 86 % compared to the inlet temperature, about 55 % compared to the heating temperature, about 6.28 % compared to the 4-cylinder model, about 12.86 % compared to the 6-cylinder model, and about 19.23 % compared to the 8-cylinder model. As the heating temperature rises to 40 °C, the overall reactor temperature for all models improves with increases of about 9.13 % for the 2-cylinder model, 13.71 % for the 4-cylinder model, 17 % for the 6-cylinder model, and 19.75 % for the 8-cylinder model. As expected, the first model with the fewest cylinders demonstrated the highest reactor temperature, while the last model with the most cylinders showed the lowest reactor temperature

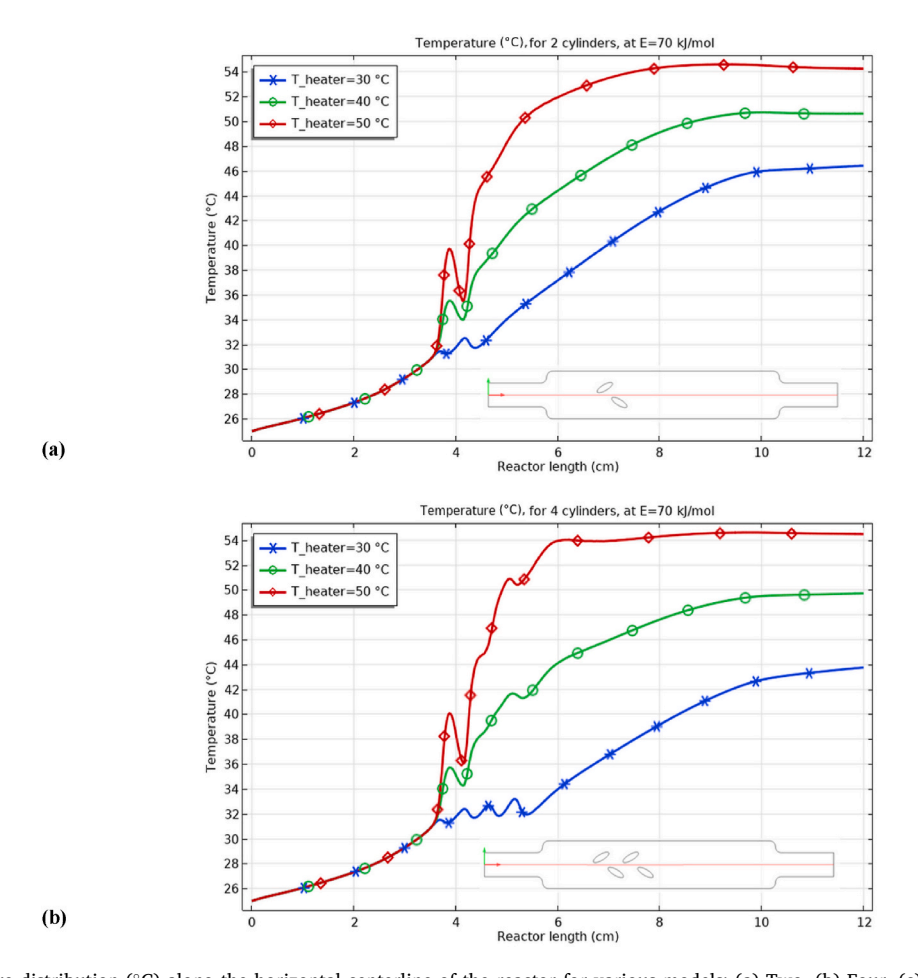


Fig. 8. Temperature distribution (°C) along the horizontal centerline of the reactor for various models: (a) Two, (b) Four, (c) Six, and (d) Eight cylinders (Combining heat from heating and exothermic reaction).

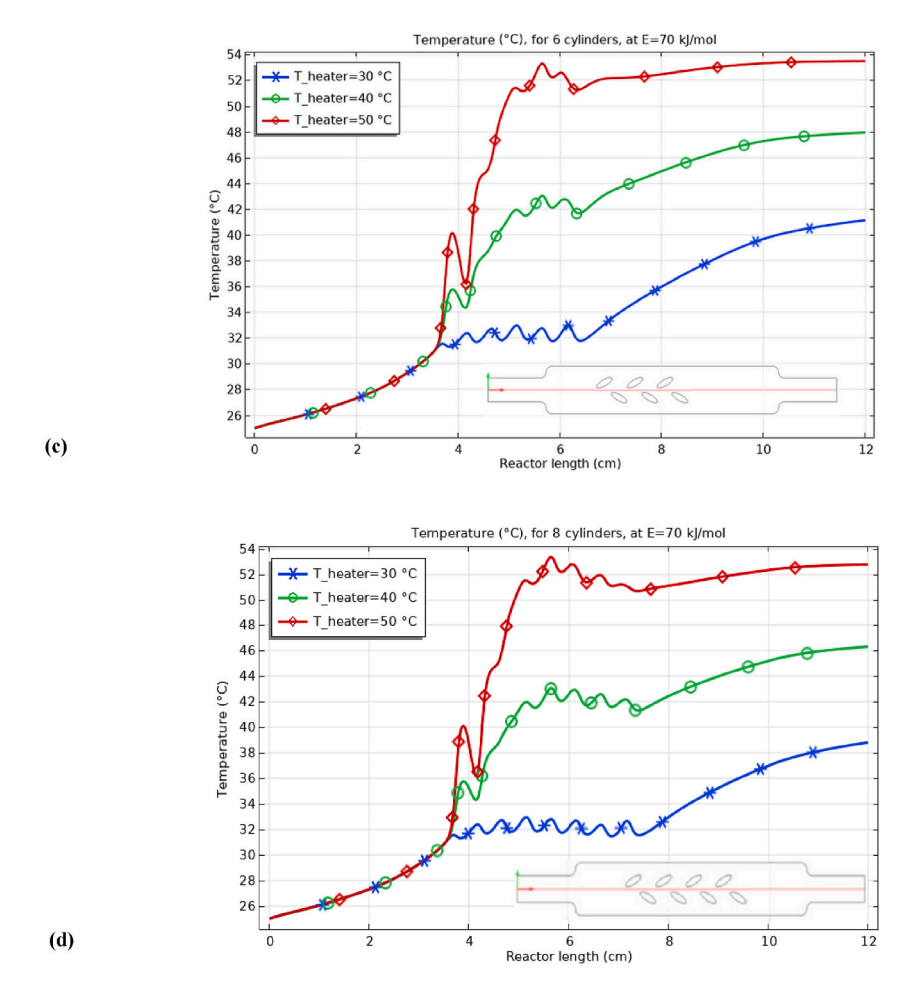


Fig. 8. (continued).

under moderate heating. At the highest heating temperature of 50 °C, the outlet temperature improves with an increase in the number of heated cylinders from 2 to 4, then decreases as the number of cylinders increases from 4 to 8. The reactor model with a moderate number of cylinders most effectively enhanced the thermal behavior of the reactor under high heating conditions.

3.3. Chemical aspects

Fig. 10 shows reaction rates in various reactor models with a different number of cylinders at various operational temperatures. For the highest temperature of 50 °C, distinct trends in the reaction rate can be differentiated by the number of cylinders inside the reactor. In the two-cylinder reactor, the reaction rates are significantly higher around the cylinders, especially on the back side of both, reaching about 26.1 mol/m^3 .s. This could be explained by the temperature increase and the resultant accelerating kinetics locally, immediately next to the heated cylinders. The reaction rate remains high in the proximity of cylinders, especially within their space, and is as much as around 25.5 mol/m^3 ·s for the case of the four-cylinder reactor. Increased surface area and more complicated flow dynamics most likely contribute to this heightened reaction rate. Indeed, the peak value of reaction rate for both the six- and eight-cylinder reactors occurs in the region involving the first four cylinders, at an estimated maximum of about 25.4 mol/m^3 ·s. After these two pairs of cylinders, the reaction rate drops to its lowest levels; thus, a saturation effect appears to be achieved where more cylinders do not significantly increase the reaction rate.

If the temperature is reduced to 40 °C, the reaction rate ranges between 13.1 and 13.3 mol/m³·s depending on the model of the reactor. The reaction zone expands towards the back walls of the cylinders; thus, a wider spatial distribution of the reaction in two- and four-cylinder reactors occurs. At 30 °C, the reaction rate further goes down to about 8.54–8.56 mol/m³·s yet again with regard to the model of the reactor. Now, the reaction zone fills nearly the whole volume of the reactor, which denotes an enormous influence of temperature upon the reaction rate and the space distribution of the reaction rate as well. It follows from obtained results that at high temperatures, reaction rate is strongly increased mainly around heated cylinders. On the other hand, lower temperatures reduce the overall reaction rate and expand the reaction zone, hence influencing the spatial dynamics in the reactor.

Fig. 11a-c depict the contours of the concentration of reactant 'A' at three different temperatures of the cylinders, 30 °C, 40 °C, and

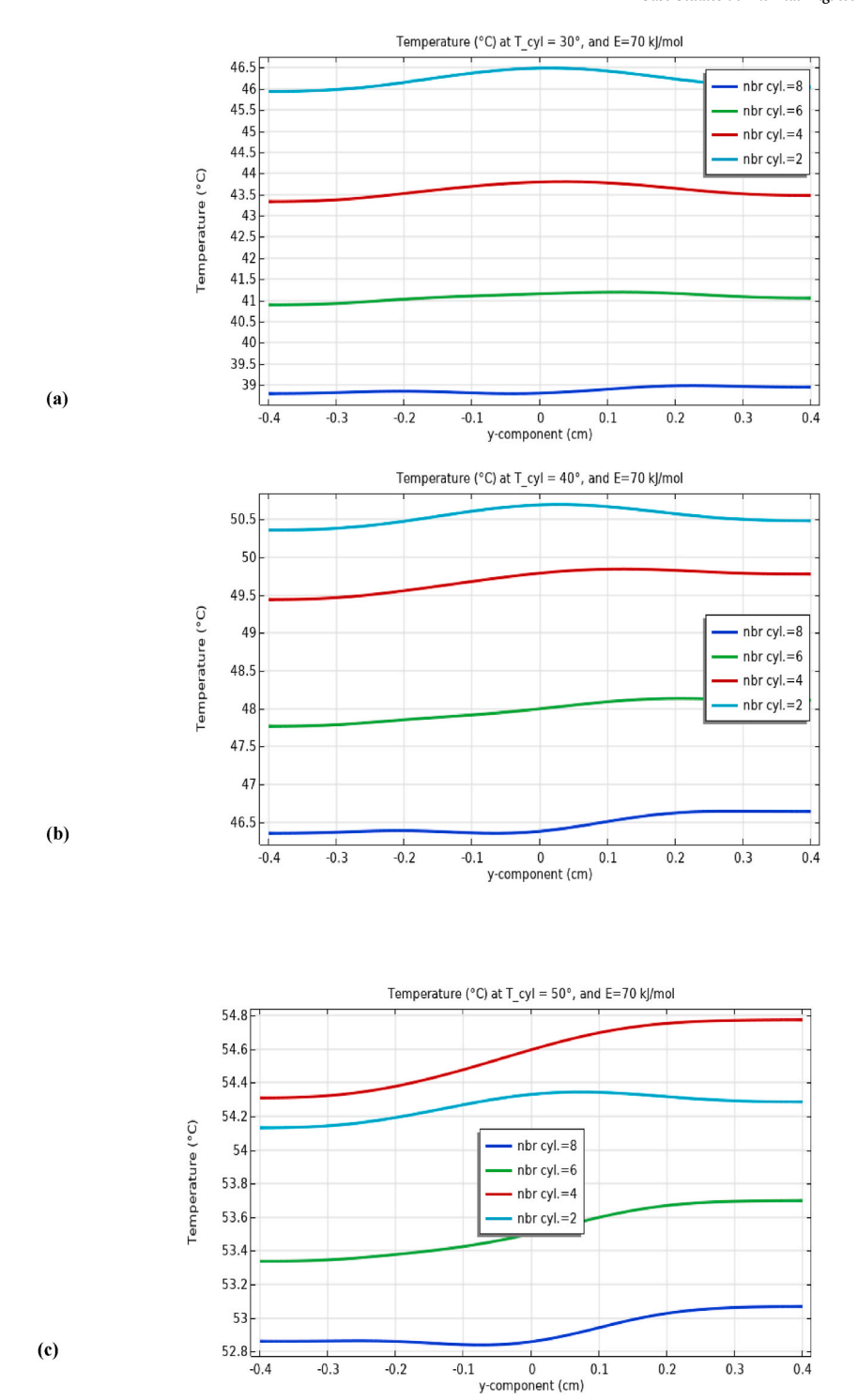


Fig. 9. Temperature distribution (°C) at the reactor exit for various models with different cylinder temperatures: (a) 30 °C, (b) 40 °C, and (c) 50 °C.

50 °C, respectively. From the results, it is observed that the decomposition rate of reactant 'A' entering the reactor at 1000 mol/m^3 increases with the rise in temperature. At 50 °C, the decomposition is very rapid as depicted by a steep gradient and a very low concentration of 'A' behind the first pair of heated cylinders. It follows that a temperature significantly enhances the kinetics of reaction hence providing faster and effective decomposition. In contrast, at 40 °C, the decomposition rate is much slower; the decrease in concentration of reactant 'A' is more gradual. The slowest decomposition occurs at 30 °C, where reactant 'A' remains in the first half of the reactor and the concentration gradient is small, indicating a limited effect on the reaction kinetics at this low temperature.

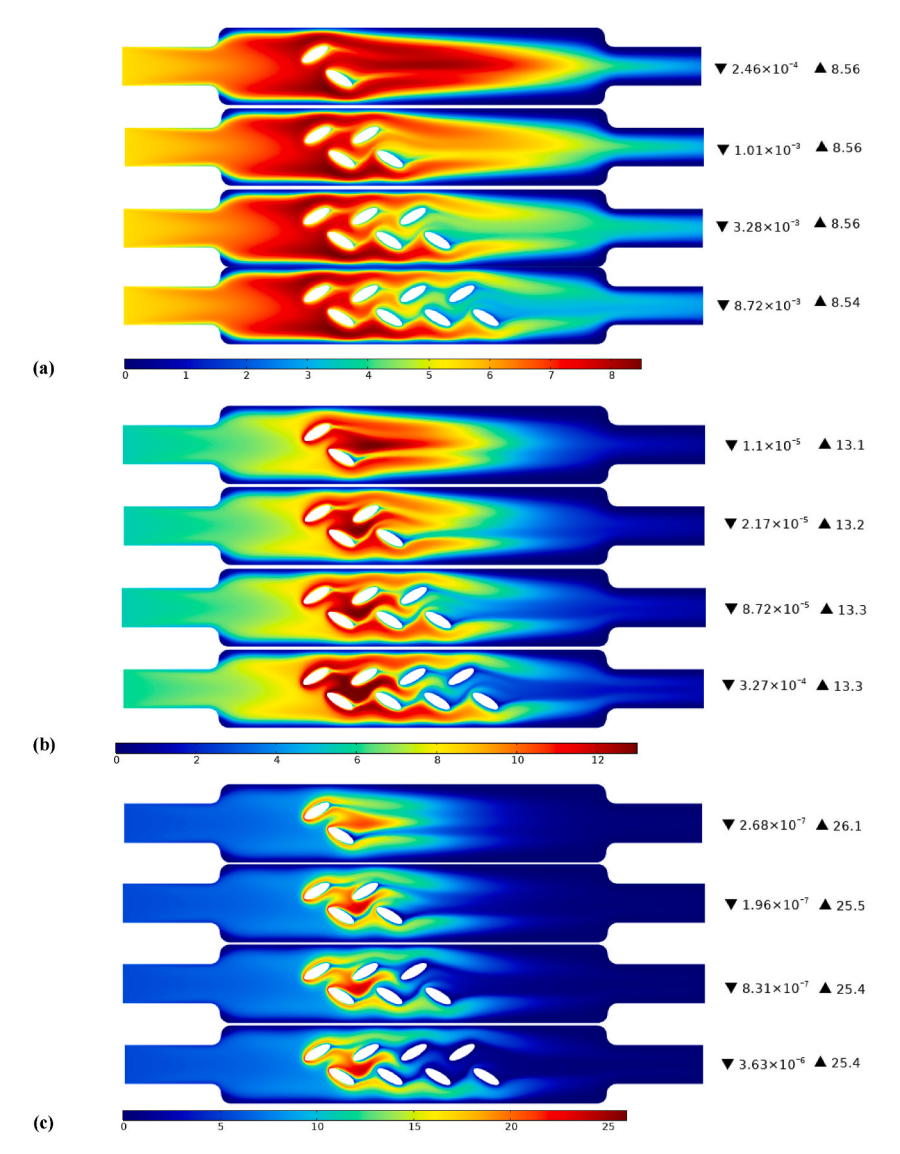


Fig. 10. Reaction rate (mol/m³.s) for different reactor models under varying cylinder temperatures: (a) T = 50 °C, (b) T = 40 °C, and (c) T = 30 °C ($R_{cyl} = 3$ mm, E = 70 kJ/mol, $V_0 = 0.001$ m/s).

The decomposition occurs most when the liquid has been heated up by the cylinder; this suggests that temperature plays a key role in the reaction. The decomposition is much slower in the front portion of the reactor, as the temperature is lower there, especially along the wall and in the downstream regions because residence times are longer there. The temperature significantly raises in the heated zone; therefore, 'A' decomposes much faster. However, even with the raised temperature, regions of relatively high concentration of 'A' still appear, which means incomplete decomposition. This is because higher water speed in the heated region reduces the residence time of the fluid in contact with the heated surfaces; therefore, the extent of decomposition is limited in this segment of the reactor.

In Fig. 12, the concentration of reactant 'A' at the reactor outlet is considered in the presence of heated cylinders. The below graph shows that by introducing more heat into the reactor through internal cylinders, reactant concentration decreases because such a high temperature will easily cause thermal decomposition of the reactant. Furthermore, the cylinders added in the reactor increased the concentration of the reactant at the outlet when the levels were $30\,^{\circ}$ C and $40\,^{\circ}$ C. On the other hand, if heating is higher, under the same conditions, there is a decrease in reactant concentration when the number of cylinders increases from 2 to 4; it increases when the number of cylinders is increased from 4 to 8. This indicates that a high level of heating increases the thermal decomposition, hence reducing the quantity of the reactant. Furthermore, the reactor with four cylinders had the lowest outlet concentration of the reactant, hence it had optimized thermal decomposition more than the other sets. This would therefore mean that the design of the reactor and the number of cylinders highly affect the rate of the reaction and the control of thermal decomposition of the reactant.

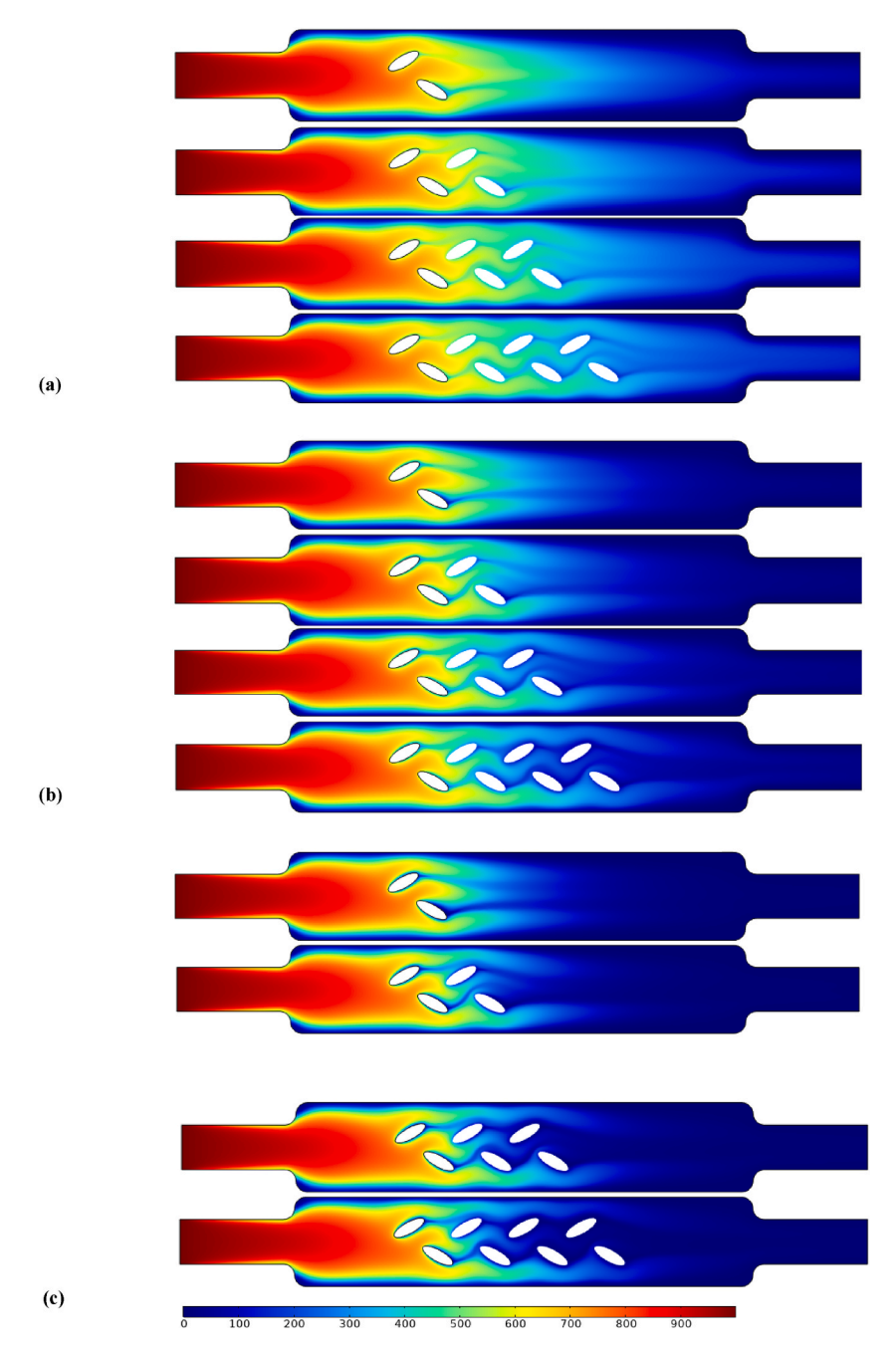


Fig. 11. Reactant 'A' concentration (mol/m³) at different cylinder temperatures: (a) T = 50 °C, (b) T = 40 °C, and (c) T = 30 °C ($R_{cyl} = 3$ mm, E = 70 kJ/mol, $V_0 = 0.001$ m/s).

3.4. Performance of the reactor

Based on the reactor performance analysis of various cylinder configurations and heating temperatures, the most optimal reactor configuration is the one with 4 cylinders at 50 $^{\circ}$ C, as shown in Table 3, that achieves a balanced performance with relatively low exit concentration of 'A', 1.0111 mol/m³, meaning high conversion efficiency of the reactant. Besides, the exit average temperature is 54.568 $^{\circ}$ C, and the rate of reaction is 25.5 mol/m³.s, which are both favorable to ensure effective thermal management and a sufficient reaction rate. Configurations with 2 cylinders at lower temperatures, such as 30 $^{\circ}$ C and 40 $^{\circ}$ C, also present competitive performance, but the 4-cylinder reactor at 50 $^{\circ}$ C provides the best compromise between high reaction rates, efficient conversion, and manageable thermal conditions, thus being the most efficient choice under the given conditions.

A 20.42 % reduction in the exit concentration of 'A' can be realized from the 4-cylinder configuration, which indicates a better

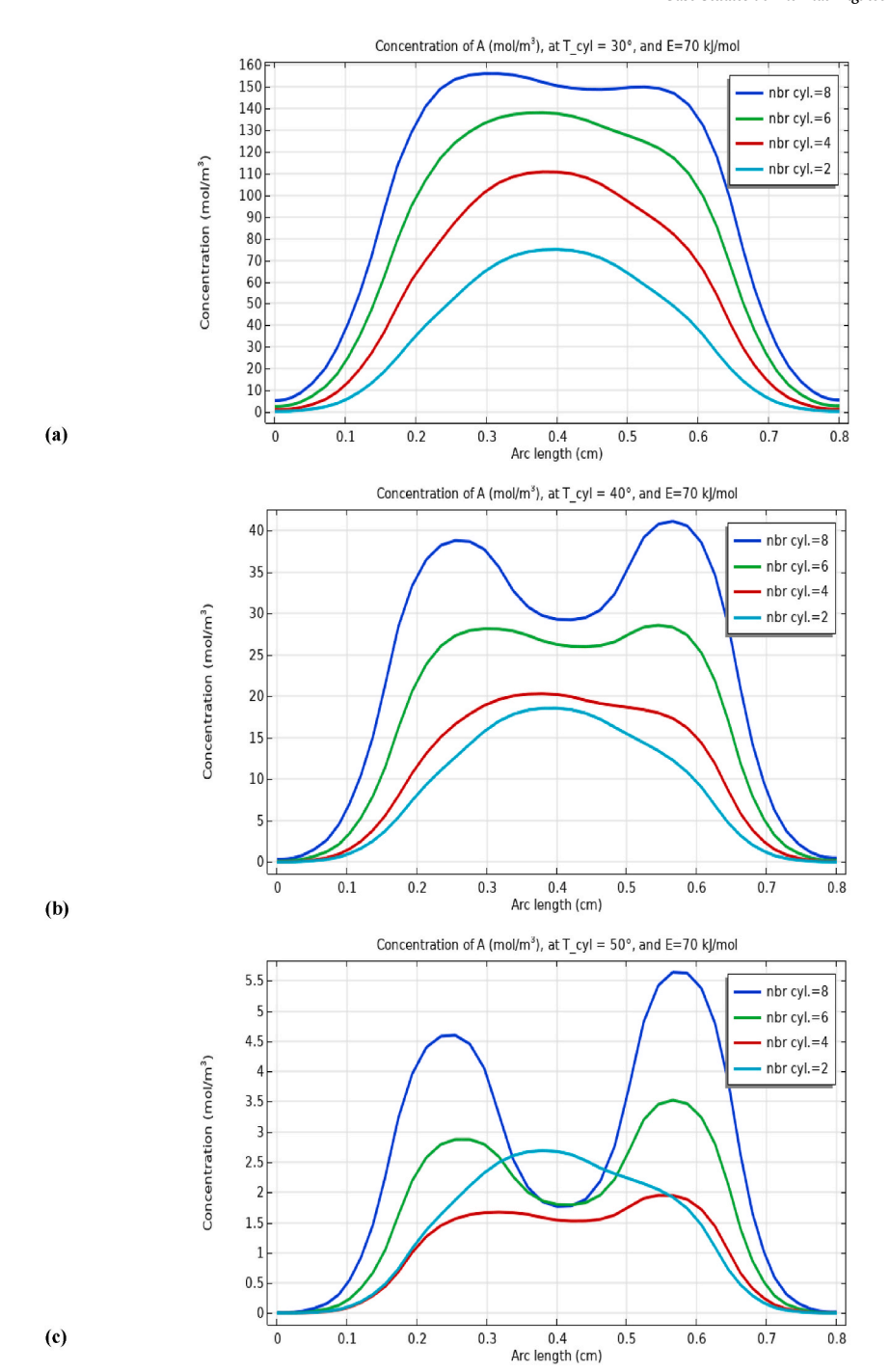


Fig. 12. Distribution of reactant 'A' concentration (mol/m³) at the reactor exit for different models with varying cylinder temperatures: (a) 30 °C, (b) 40 °C, and (c) 50 °C.

conversion of reactants compared to the 2-cylinder reactor configuration. While the rate of reaction is lower by 2.29 %, the 4-cylinder configuration has a slightly higher exit temperature by 0.56 %. Compared to the 6- cylinder reactor, the 4- cylinder configuration gives a marginal 0.39 % increase in reaction rate and a significant 39.59 % decrease in exit concentration of 'A'. Exit temperature is higher by 1.96 % in the case of the 4-cylinder configuration; therefore, thermal management is good in this configuration. Finally, with respect to the 8-cylinder reactor, the 4-cylinder arrangement shows a 0.39 % increase in the rate of reaction and a 59.90 % decrease in the exit concentration of 'A', while being 3.11 % higher in terms of exit temperature. Overall, these results point to the 4-cylinder reactor at 50 °C as the most efficient configuration regarding reactant conversion and thermal conditions.

Table 3 Reactor performance parameters for different cylinder configurations ($R_{cyl} = 3$ mm, E = 70 kJ/mol, $V_0 = 0.001$ m/s).

Number of Cylinders	T _{cyl} (°C)	Exit average temperature (°C)	Rate of reaction (mol/m ³ .s)	Exit average concentration of 'A' (mol/m ³)
4	50	54.568	25.5	1.0111
2		54.262	26.1	1.2707
6		53.517	25.4	1.674
8		52.928	25.4	2.5204
2	40	50.542	13.1	8.7094
4		49.696	13.2	10.978
6		47.981	13.3	17.15
8		46.471	13.3	23.843
2	30	46.215	8.56	36.111
4		43.593	8.56	58.571
6		41.077	8.56	81.388
8		38.875	8.54	101.08

3.5. Effect of the cylinder size

This section deals with the investigation of a reactor's performance due to size variation of heated cylinders. An optimum reactor with four hot cylinders at 50 °C is considered; this optimum reactor will be analyzed in terms of variations of the radius, $R_{cyl} = 2$ mm, 3 mm and 4 mm. The temperature of the reactor is considered within this analysis for a fixed value of the inlet velocity at 0.001 m/s with an activation energy of 70 kJ/mol. As shown in Fig. 13, the reactor temperature is very important in the second half of the reactor where it improves as the cylinder size increases from 1 mm to 3 mm due to the increase in the size of the heated surfaces.

Fig. 14 presents the reaction rate analysis. It follows that the reaction rate enhances significantly around the heated cylinders because this region possesses the highest temperatures to augment thermal decomposition. Therefore, it can be seen that the reaction rate in both small and large diameters of the cylinders is very large, which indicates that the change in cylinder size affects the reaction rate. Moreover, the concentration of the reactant 'A' is analyzed, as shown in Fig. 15. The reactant concentration in the first half of the reactor is high but significantly goes down near the heated cylinders and in the second half of the reactor. The greater the size of the cylinder, the lower the concentration of the reactant, since its decomposition rate increases with increased area of heating.

In order to find the optimal value of the cylinder size for the reactors in the four-cylinder model, exit average temperature, rate of reaction, and exit average concentration of 'A' are presented in Table 4. The temperatures at the exit for the R_{cyl} sizes of 2 mm, 3 mm, and 4 mm are 53.412 °C, 54.568 °C, and 56.332 °C, respectively. Thus, $R_{cyl} = 4$ mm resulted in a temperature which was 5.46 % higher with respect to $R_{cyl} = 2$ mm and 3.23 % higher with respect to $R_{cyl} = 3$ mm and can be taken as better conversion efficiency. The corresponding rates of reaction for the R_{cyl} sizes of 2 mm, 3 mm, and 4 mm are 27.5 mol/m³.s, 25.5 mol/m³.s, and 26.1 mol/m³.s respectively. Even though $R_{cyl} = 2$ mm has the highest rate, $R_{cyl} = 4$ mm has a rate only 5.09 % lower while $R_{cyl} = 3$ mm is 7.27 % lower. These show that the rates at 3 mm and 4 mm remain competitive. The respective values of exit concentrations of 'A' for R_{cyl} sizes 2 mm, 3 mm, and 4 mm are 1.7703 mol/m³, 1.0111 mol/m³, and 0.44902 mol/m³, respectively. The value for $R_{cyl} = 4$ mm shows a decrease of about 74.63 % concentration from $R_{cyl} = 2$ mm, and that of $R_{cyl} = 3$ mm also about 55.59 %. It is concluded that $R_{cyl} = 4$ mm has the highest conversion of reactant 'A' to products. Since the factors are balancing each other, $R_{cyl} = 4$ mm will be an optimum size considering highest exit average temperature, competitive rate of reaction, and extremely lower exit concentration of 'A' assuming outstanding overall performance in the reactor model.

4. Conclusions

This paper examines thermal decomposition performance in cylindrical reactors, highlighting the crucial effect of reactor configuration and heating conditions on the efficiency of thermosensitive and exothermic reactions. This work determines the most effective setup by analyzing reactors with a different number of heated cylinders at different temperatures, from 2, 4, 6, and 8 cylinders at 30 $^{\circ}$ C, 40 $^{\circ}$ C, and 50 $^{\circ}$ C.

Key findings show that the 4-cylinder reactor, heated to 50 °C, presents the best balance of high reactant conversion, effective

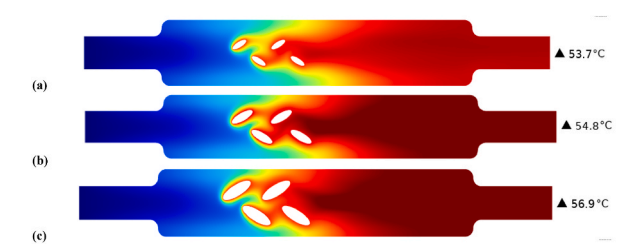


Fig. 13. Temperature distribution (°C) in a four-cylinder reactor for different cylinder sizes: (a) $R_{cyl} = 2$ mm, (b) $R_{cyl} = 3$ mm, and (c) $R_{cyl} = 4$ mm ($T_{cyl} = 50$ °C, E = 70 kJ/mol, $V_0 = 0.001$ m/s).

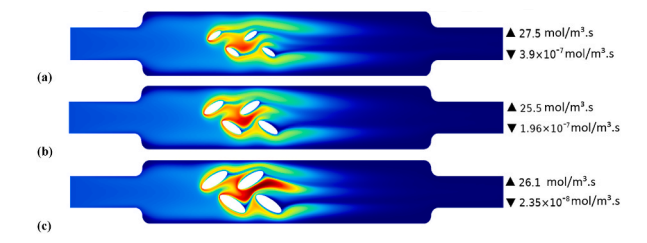


Fig. 14. Reaction rate distribution (mol/m³.s) in a four-cylinder reactor for different cylinder sizes: (a) $R_{cyl} = 2$ mm, (b) $R_{cyl} = 3$ mm, and (c) $R_{cyl} = 4$ mm ($T_{cyl} = 50$ °C, E = 70 kJ/mol, $V_0 = 0.001$ m/s).

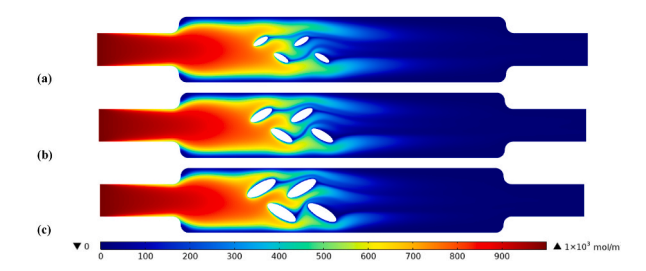


Fig. 15. Reactant 'A' concentration (mol/m³) in a four-cylinder reactor for different cylinder sizes: (a) $R_{cyl} = 2$ mm, (b) $R_{cyl} = 3$ mm, and (c) $R_{cyl} = 4$ mm ($T_{cyl} = 50$ °C, E = 70 kJ/mol, $V_0 = 0.001$ m/s).

Table 4 Performance parameters of reactors with varying cylinder sizes in a four-cylinder model ($T_{cyl} = 50$ °C, $V_0 = 0.001$ m/s, E = 70 kJ/mol).

Number of Cylinders	R _{cyl} (mm)	Exit average temperature (°C)	Rate of reaction (mol/m ³ .s)	Exit average concentration of 'A' (mol/m ³)
4	2	53.412	27.5	1.7703
	3	54.568	25.5	1.0111
	4	56.332	26.1	0.4490

thermal management, and efficient reaction rates. The configuration gave a low exit concentration of reactant 'A' (1.0111 mol/m^3) , a high average exit temperature (54.568 °C), and a favorable reaction rate (25.5 mol/m 3 .s). When the comparisons are made amongst many, the 4-cylinder reactor at 50 °C gives a much smaller exit concentration of reactant 'A', improved thermal condition, and competitive values for reaction rates.

Further optimization of the cylinder size in the optimal configuration of 4 cylinders, showed that increasing the cylinder radius to a radius of 4 mm gave the best conversion efficiency, with a 74.63 % reduction in the exit concentration of 'A', compared with a 2 mm radius, while still maintaining competitive reaction rates. Therefore, the reactor with four cylinders of 4 mm radius heated up to $50\,^{\circ}$ C is concluded as the most efficient configuration in order to enhance thermal decomposition processes.

Numerical results obtained are very helpful in the design and optimization of cylindrical reactors for thermal decomposition applications, as the number, temperature of heating, and dimensions of cylinders have to be selected appropriately to reach optimum performance.

Future research will be conducted to study the effect of extra geometric parameters on performance. The spacing of cylinders is to be optimized and the effects of cylinder arrangement: staggered and inline have to be investigated, while varying the angle of inclination. Each of the above-mentioned factors shall be studied methodically for their contribution towards the efficiency and performance of the overall system.

CRediT authorship contribution statement

Djelloul Bendaho: Writing – review & editing, Writing – original draft, Methodology, Investigation, Conceptualization. Zakaria Sari Hassoun: Writing – review & editing, Writing – original draft, Methodology, Investigation, Conceptualization. Noureddine Kaid: Writing – review & editing, Writing – original draft, Methodology, Investigation, Conceptualization. Sultan Alqahtani: Writing – review & editing, Writing – original draft, Methodology, Investigation, Conceptualization. Younes Menni: Writing – review & editing, Writing – original draft, Methodology, Investigation, Conceptualization. Ali J. Chamkha: Writing – review & editing, Writing – original draft, Methodology, Investigation, Conceptualization. Badr M. Alshammari: Writing – review & editing, Writing – original draft, Methodology, Investigation, Conceptualization. Lioua Kolsi: Writing – review & editing, Writing – original draft, Methodology, Investigation, Conceptualization. Conceptualization. Conceptualization. Conceptualization. Conceptualization.

Declaration of competing interest

The authors declare that they have no known competing financial interests or personal relationships that could have appeared to influence the work reported in this paper.

Acknowledgments

The authors extend their appreciation to the Deanship of Research and Graduate Studies at King Khalid University for funding this work through Large Research Project under grant number RGP2/352/45.

Data availability

Data will be made available on request.

References

- [1] M. Ferus, G. Cassone, V. Táborský, A. Heays, L. Petera, A. Knizek, S. Civiš, Thermal decomposition of cocaine and methamphetamine investigated by infrared spectroscopy and quantum chemical simulations, ACS Omega 6 (22) (2021) 14447–14457, https://doi.org/10.1021/acsomega.1c01325.
- [2] H. Kwon, G. Mpourmpakis, Ab initio thermochemistry of highly flexible molecules for thermal decomposition analysis, J. Chem. Theor. Comput. 19 (12) (2023) 3652–3663, https://doi.org/10.1021/acs.jctc.3c00265.
- [3] S. Ghosh, D. Pal, Mathematical modelling of a non-isothermal tubular reactor, Current Mater. Sci.: Formerly: Recent Patents on Mater. Sci. 15 (3) (2022) 280–294. https://doi.org/10.2174/2666145415666220411084657.
- [4] R.S. Lebelo, M. Waetzel, R.K. Mahlobo, K.C. Moloi, S.O. Adesanya, On transient heat analysis of a two-step convective reactive cylinder, J. Phys. Conf. 1730 (2021) 012141, https://doi.org/10.1088/1742-6596/1730/1/012141.
- [5] R.S. Lebelo, O.D. Makinde, Two-Step exothermic chemical reaction for heat transfer investigation in a convective cylinder, in: J. Xu, K.M. Pandey (Eds.), Mechanical Engineering and Materials. Mechanisms and Machine Science, vol. 100, Springer, Cham, 2021, https://doi.org/10.1007/978-3-030-68303-0_5
- [6] A.R. Hassan, H.A. Ogunseye, J.A. Gbadeyan, The thermal analysis in a cylindrical pipe with surface cooling and possible heat loss, J. Energetic Mater. 37 (1) (2019) 57–69, https://doi.org/10.1080/07370652.2018.1522391.
- [7] L. Vernieres-Hassimi, R. El Assoudi-Baikari, M.A. Abdelghani-Idrissi, N. Mouhab, New analytical method for maximum temperature assessment in an exothermic tubular chemical reactor, Chem. Eng. Commun. 203 (2) (2016) 174–181, https://doi.org/10.1080/00986445.2014.973943.
- [8] R.S. Lebelo, Transient heat and reactant consumption investigation in a cylindrical pipe of variable thermal conductivity, Defect Diffusion Forum 392 (2019) 178–188. https://doi.org/10.4028/www.scientific.net/DDF.392.178. Trans Tech Publications Ltd.
- [9] N.K. Lamba, Thermosensitive response of a functionally graded cylinder with fractional order derivative, Int. J. Appl. Mech. Eng. 27 (1) (2022) 107–124, https://doi.org/10.2478/ijame-2022-0008.
- [10] V. Makkar, K. Dang, N. Sharma, S. Yadav, Numerical investigation of MHD convective free stream nanofluid flow influenced by radiation and chemical reaction over stretching cylinder, Heat Transfer 52 (3) (2023) 2328–2347, https://doi.org/10.1002/htj.22786.
- [11] G.A. Rios, J. Sebastián Rincón Tabares, A. Montoya, D. Restrepo, H. Millwater, Transient thermomechanical sensitivity analysis using a complex-variable finite element method, J. Therm. Stress. 45 (5) (2022) 341–374, https://doi.org/10.1080/01495739.2022.2049022.
- [12] F. Alzahrani, S.A. Khan, M.U. Rahman, M.I. Khan, Entropy optimized chemical reactive flow of nanofluid subjected to a stretchable cylinder, Int. J. Mod. Phys. B 38 (9) (2024) 2450126. https://doi.org/10.1142/S0217979224501261.
- [13] Y.J. Lim, S. Shafie, S.M. Isa, N.A. Rawi, A.Q. Mohamad, Impact of chemical reaction, thermal radiation and porosity on free convection Carreau fluid flow towards a stretching cylinder, Alex. Eng. J. 61 (6) (2022) 4701–4717, https://doi.org/10.1016/j.aej.2021.10.023.
- [14] N. Chandra Roy, R.S. Reddy Gorla, Natural convection of reacting chemical in square enclosure with circular cylinder, J. Thermophys. Heat Tran. 36 (3) (2022) 507–519, https://doi.org/10.2514/1.T6298.
- [15] M. Zhang, Y. Li, E. Uchaker, S. Candelaria, L. Shen, T. Wang, G. Cao, Homogenous incorporation of SnO₂ nanoparticles in carbon cryogels via the thermal decomposition of stannous sulfate and their enhanced lithium-ion intercalation properties, Nano Energy 2 (5) (2013) 769–778, https://doi.org/10.1016/j.nanoen.2013.01.009
- [16] W. Wijayanti, M.N. Sasongko, S. Sasmoko, A thermolysis of macroalgae gracilaria affected by temperature pyrolysis, AIP Conf. Proc. 2097 (2019) 030047, https://doi.org/10.1063/1.5098222.
- [17] A.E. Thomas, B.J. Cantwell, Hypergolic reaction and thermal decomposition of an ionic liquid, in: 2018 Joint Propulsion Conference, 2018, p. 4963, https://doi.org/10.2514/6.2018-4963.
- [18] R. Polanský, P. Prosr, P. Hahn, Changes in the Activation Energy of Thermal Decomposition of Mineral Oil during Accelerated Thermal Ageing, 2018 IEEE 2nd International Conference on Dielectrics (ICD), Budapest, Hungary, 2018, pp. 1–4, https://doi.org/10.1109/ICD.2018.8514753, 2018.
- [19] A.A. Onischuk, V.P. Strunin, M.A. Ushakova, V.N. Panfilov, Studying of silane thermal decomposition mechanism, Int. J. Chem. Kinet. 30 (2) (1998) 99–110, https://doi.org/10.1002/(SICD)1097-4601(1998)30:2<99::AID-KIN1>3.0.CO:2-O.
- [20] H. Nagasawa, M. Maruyama, T. Komatsu, S. Isoda, T. Kobayashi, Physical characteristics of stabilized silver nanoparticles formed using a new thermal-decomposition method, Phys. Status Solidi 191 (1) (2002) 67–76, https://doi.org/10.1002/1521-396X(200205)191:1<67::AID-PSSA67>3.0.CO;2-M.
- [21] F. Kubatovics, M. Blazsó, Thermal decomposition of polyamide-6 in the presence of PVC, Macromol. Chem. Phys. 201 (3) (2000) 349–354, https://doi.org/10.1002/(SICD1521-3935(20000201)201:3-349::AID-MACP349>3.0.CO:2-V.
- [22] M. Kohga, Thermal decomposition behavior and burning characteristics of ammonium nitrate/polytetrahydrofuran propellants with glycerol propoxylate as a crosslinking agent, in: AIAA Propulsion and Energy 2019 Forum, 2019, p. 4364, https://doi.org/10.2514/6.2019-4364.
- [23] A.Z. Kaltaev, K.B. Larionov, S.A. Yankovsky, K.V. Slyusarsky, V.E. Gubin, Production of black carbon by steam pyrolysis (thermolysis) method of rubber waste in the form of worn-out automobile tires, AIP Conf. Proc. 2212 (2020) 020023, https://doi.org/10.1063/5.0000970.
- [24] D. Bendaho, N. Kaid, S. Alqahtani, B.M. Alshammari, Y. Menni, A.J. Chamkha, L. Kolsi, CFD-aided enhancement of propylene oxide decomposition in a tubular reactor with a corrugated cooling jacket, Case Stud. Therm. Eng. 61 (2024) 105004, https://doi.org/10.1016/j.csite.2024.105004.

Nomenclature

Symbol Definition Units *A*: Pre-exponential factor l/s *A*: Chemical Compound

- *B*: Chemical Compound c_A : Concentration of compound 'A' mol/m³
- *Ci:* Concentration of species *i* mol/m³
- C. Concentration of species *i* mol/m³ Cp: Specific heat capacity J/(kg.K)
 d: Characteristic diameter m
 D: Diffusion coefficient of species *i* m²/s

- E: Activation energy J/mol
- F: Body force term N/m³
- H: Heat of reaction kJ/mol
 k: Speed coefficient (or speed constant)
- λ: Thermal conductivity W/(m.K)
- n: Outward-pointing unit normal vector
- Ni: Mass flux of species i kg/(m² s) Nu: Nusselt number
- P: Pressure Pa
- Q: Rate of energy release (heat source or sink) W/m³
- R: Gas constant 8.314 J/(mol·K)
- Ri: Reaction rate of species $i \text{ mol/(m}^3 \cdot \text{s})$ Re: Reynolds number
- T: Temperature °C
- T_0 : Inlet temperature °C
- *Tcyl:* Cylinder temperature °C
- t: Time s
- u: Velocity vector m/s
- u₀: Boundary velocity m/s
- μ: Dynamic viscosity Pa.s
 ρ: Fluid density kg/m³
- h: Convective heat transfer coefficient W/m².K